9th IAA Planetary Defense Conference – PDC 2025
5–9 May 2025, Stellenbosch, Cape Town, South Africa

IAA-PDC25-01-212

ANALYSIS OF ASTEROID DEFLECTION MISSION OPTIONS FOR THE 2025 PLANETARY DEFENSE CONFERENCE HYPOTHETICAL ASTEROID IMPACT THREAT SCENARIO BY THE ITALIAN SPACE AGENCY DELEGATION AT SMPAG

S. Franzese[a,1,*], E. Basile[a,2,*], E. M. Polli[a,1], C. Colombo[a,3], P. Vasiliki[b,4], M. Castronuovo[b,4], J. L. Cano[c,5]

[a] *Politecnico di Milano, Dipartimento di Scienze e Tecnologie Aerospaziali (DAER), Via La Masa 34, Milano, 20156, Italy*
[b] *Italian Space Agency, Via del Politecnico, Roma, 00133, Italy*
[c] *ESA - ESOC / Planetary Defence Office, Robert-Bosch-Straße 5, 64293, Darmstadt, Germany*

Abstract

The growing interest in addressing asteroid threat scenarios is justified by current estimates of the Potentially Hazardous Objects (PHOs) population and by recent impacts on Earth. This paper presents and analyses preliminary mission design options for the mitigation of asteroid 2024 PDC25, focus of the hypothetical impact threat scenario introduced for the Planetary Defense Conference 2025.
Specifically, both a reconnaissance mission and deflection campaigns with different deviation strategies are proposed. The developed impulsive fast flyby reconnaissance mission allows for the enhancement of the estimation of asteroid 2024 PDC25's physical properties. The Multiple Kinetic Impactor (MKI) and Nuclear Explosive Devices (NEDs) in a "Carrier" configuration are selected and analysed as impulsive deflection alternatives. Models for the Standard and Enhanced Gravity Tractor (GT), Single and Multiple Laser Ablation (LA), Single Ion Beam Deflection (IBD) and a newly developed technique of Multiple IBD in Formation Flying are developed as continuous slow push/pull deviation strategies. The selection of these strategies was mainly based on a sufficiently high Technology Readiness Level (TRL), enabling near-term applications if their development is prioritised. Being the Kinetic Impactor strategy the only flight-proven technology, uncertainties in various parameters are also incorporated into the model developed for the MKI.
Deflection campaigns with the analysed techniques and different timelines are proposed to divert asteroid 2024 PDC25 from a collision course with Earth. A final comparison is conducted among the proposed mitigation options, based on their deflection performance, technological readiness and feasibility within the available warning time. Based on this assessment, the most effective strategies to deflect asteroid 2024 PDC25 are identified as MKI, stand-off NEDs in "Carrier" configuration and MIBD.

Keywords: PHOs, deflection strategies, momentum enhancement, preliminary design

*Corresponding author
Email addresses: saverio.franzese@mail.polimi.it (S. Franzese), elena1.basile@mail.polimi.it (E. Basile), eduardomaria.polli@polimi.it (E. M. Polli), camilla.colombo@polimi.it (C. Colombo), vasiliki.petropoulou@asi.it (P. Vasiliki), marco.castronuovo@asi.it (M. Castronuovo), Juan-Luis.Cano@esa.int (J. L. Cano)
[1] Mr., Politecnico di Milano - DAER
[2] Ms., Politecnico di Milano - DAER
[3] Dr., Politecnico di Milano - DAER
[4] Dr., ASI
[5] Mr., ESA - ESOC

1. Introduction

The potential impact threat posed by Near-Earth Objects (NEOs) demonstrates the need to enhance planetary defence techniques, to ensure preparedness in case a real collision hazard is ever discovered. Since 2015, exercises involving hypothetical hazardous asteroids have been proposed, with various solutions discussed during Planetary Defense Conferences (PDCs). This paper presents and analyses preliminary mission design options for the mitigation of asteroid "2024 PDC25", focus of the hypothetical impact threat scenario introduced for the PDC 2025.

An impulsive fast flyby reconnaissance mission is proposed to improve knowledge of the asteroid's physical and orbital properties and inform the design of deflection campaigns. Then, this work focuses on developing several alternatives for diverting asteroid 2024 PDC25 from a collision course with Earth, based on both impulsive and slow push/pull techniques.

Among the impulsive techniques, the Kinetic Impactor (KI) has the highest Technology Readiness Level (TRL), demonstrated by the Double Asteroid Redirection Test (DART) mission [1]. It is a conceptually simple strategy, requiring no landing or attachment. However, its effectiveness is highly sensitive to the asteroid's composition and internal structure [2]. Building on the flight-proven Single KI, the Multiple KI (MKI) strategy [3] uses a sequence of impacts from multiple spacecraft to improve deflection performance. This strategy remains unproven in space and shares the KI's sensitivity to the asteroid's properties.

Less technically mature strategies have demonstrated to be effective in deviating asteroid 2024 PDC25. Therefore, this work also focuses on the implementation, from previous literature, and improvement of models for deflection strategies with a lower TRL compared to the kinetic impactor, but still viable for near-term applications if their development is prioritised.

Specifically, Nuclear Explosive Devices (NEDs) are a valid impulsive alternative to kinetic impactors, offering the highest energy density among all deflection techniques [4]. Leveraging the Nuclear Cycler approach proposed in [5], a model is implemented for stand-off NEDs in a "Carrier" configuration.

Given the warning time available in this scenario, models of slow push/pull deflection strategies are also developed. The considered techniques include the Standard and Enhanced Gravity Tractor (GT and EGT), conceptually proposed in [6] and [7] respectively; Single and Multiple Laser Ablation (SLA and MLA), leveraging the work done in [8] and [9]; Single and Multiple Ion Beam Deflection (SIBD and MIBD), following the concept proposed in [10].

In this study, the models developed for the different deflection techniques include improvements with respect to previous literature. Specifically, for the MKI strategy, uncertainties in key parameters are incorporated into the model to enable robust mission design. For the other techniques, the improvements focus on refining the deflection models and exploiting different proximity configurations, while ensuring a feasible spacecraft design for each mission. The approach adopted in this work follows previous studies aiming at optimising the deflection mission's performances [11]. In particular, the models for the various mitigation strategies are integrated into a multi-objective optimisation process to allow for the identification of viable alternatives for asteroid 2024 PDC25 deflection. MATLAB's *gamultiobj*, a specific implementation of a multi-objective Genetic Algorithm (GA), is employed for addressing the competing objectives of maximising b-plane deflection, minimising warning time and total mass at launch, while ensuring spacecraft design feasibility. The optimisation allows for the identification of Pareto-optimal solutions. All the solutions belonging to the Pareto sets are associated with bounded optimisation variables and are forced to satisfy optimisation constraints.

A final comparison is conducted among the proposed mitigation options, based on their deflection performance, technological readiness and feasibility within the available warning time. Based on this assessment, the most effective strategies to deflect asteroid 2024 PDC25 are identified as the MKI, the stand-off NEDs in "Carrier" configuration, and the MIBD.

2. Asteroid 2024 PDC25 properties and reconnaissance

Asteroid 2024 PDC25 is a fictitious NEO, focus of the hypothetical impact threat scenario specifically designed for in-depth discussion at the International Academy of Astronautics (IAA) 2025 Planetary Defense Conference in Stellenbosch (Cape Town), South Africa. The estimated impact probability for asteroid 2024 PDC25 surpassed the International Asteroid Warning Network (IAWN) notification threshold of 1 % in late July 2024. As a result, an official warning was issued on 1^{th} August 2024, referred to as Epoch 1 [12].

At Epoch 1, asteroid 2024 PDC25 is classified as an S-type [12]. The asteroid's diameter is most likely

within the range of 90 - 160 m, with a median estimate of 125 and measurements extending from 50 m to 280 m [12]. As an outcome of the analyses started by SMPAG at Epoch 1, the first step for the mitigation of the threat posed by asteroid 2024 PDC25 would be the implementation of a flyby reconnaissance mission. This would largely improve the knowledge of the physical properties of the asteroid, mainly regarding its size and shape.
In this work, the mission analysis for a fast flyby reconnaissance mission is proposed. The design of this mission is based on a grid-search approach, in which the available departure and arrival windows are selected as a compromise between the mission design timeline requirements and the need for the reconnaissance data to be available as soon as possible. In particular, the first launch date is considered not earlier than 3 years after the IAWN's impact probability threshold is met, and the grid search is successively refined around the 2027 launch and 2028 arrival windows. The resulting trajectory of the reconnaissance spacecraft is shown in Figure 1. The designed mission involves a launch scheduled for the 2^{nd} of September 2027, with an arrival predicted for the 31^{st} of March 2028.

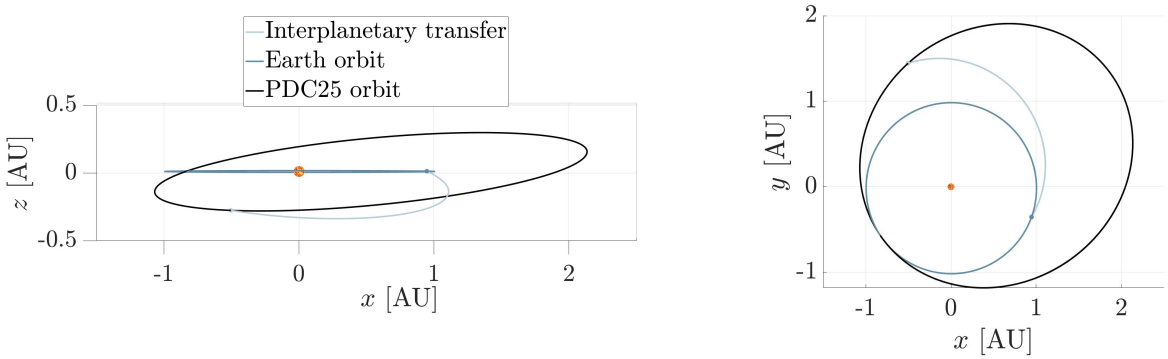

(a) Side view (b) Upper view

Figure 1: Interplanetary trajectory for the fast flyby reconnaissance mission.

Epoch 2 represents a point in time nearly four years after Epoch 1, aligning with the moment when data from the flyby reconnaissance mission become available. By this stage, it is confirmed that asteroid 2024 PDC25 is on a collision course with Earth, with impact predicted for 24th April 2041, which is 13 years after Epoch 2. As an outcome of the reconnaissance mission, the asteroid is found to have an elongated shape, approximately twice as long as it is wide, with a spherical equivalent diameter ranging from 145 to 155 m [12]. In this work, the statistical distributions provided for the asteroid's physical properties [12] are utilised in distinct ways, depending on the deflection strategy under consideration.

2.1. B-plane deflection requirements

The performances of the deflection strategies are compared in terms of deviation on the b-plane. At Epoch 1, the required deflection for the mission to be considered successful must be the entire gravitational capture cross-section of Earth in the b-plane, corresponding to the full length of the impact risk chord, $C = 21850$ km. At Epoch 2, however, the region of possible impact locations is reduced, allowing for a more precise definition of deflection requirements. Asteroid 2024 PDC25 can be deflected either northward or southward. The northward deflection requirement in terms of impact parameter is approximately $0.34\,C$ (or equivalently $1.16\,R_E$), and it is lower than the southward one, which is about $0.70\,C$ (or $2.41\,R_E$). However, a northward deflection would redirect the asteroid towards more densely populated regions. Conversely, although it requires twice the deflection, the southward deflection offers the advantage of redirecting the asteroid through fewer countries and towards the Southern Ocean. This is particularly beneficial in case a full deflection is not achievable, as the impact would occur on the ocean, where, for asteroids of this size, the resulting tsunamis are unlikely to pose a global threat [13].
For kinetic impactors, a southward deflection is the only feasible alternative: a northward deflection, which implies imparting impulses in the opposite direction as the asteroid's velocity, would require placing one or more spacecraft on a highly energetic orbit. All other deflection strategies analysed in this work can alter the asteroid's orbit either southward or northward by applying a perturbing acceleration in the same or opposite direction of its velocity vector. This results from the use of a low-thrust trajectory, which allows the spacecraft to rendezvous with the asteroid and apply the perturbing forces in any preferential direction.

3. Multiple Kinetic Impactor strategy

The KI strategy involves a direct collision between an impactor spacecraft and the asteroid, transferring momentum to instantaneously alter its orbit. Exploiting multiple impactors reduces the risk of fragmentation by imparting smaller impulses to the asteroid, while still allowing for effective deflection. For the specific case of the MKI strategy, a nominal deflection scenario is identified in accordance with a baseline model representative of the asteroid. Successively, varying conditions are subsequently incorporated in the nominal design, including changes in the asteroid's physical properties and heliocentric position, and navigation errors. The resulting sensitivity analysis allows for a robust MKI mission design for 2024 PDC25.

3.1. Nominal MKI mission design

The asteroid is assumed to be non-rotating, homogeneous and spherical, with its density (ρ_{ast}) and diameter (d_{ast}) coincident with the mean values of the respective after-reconnaissance distributions. The momentum enhancement due to the generation of the ejecta plume after the impact is modelled by exploiting a multiplicative momentum enhancement factor (β) applied to the impact-induced velocity variation of the asteroid. The value of the momentum enhancement factor is selected based on the Double Asteroid Redirection Test mission outcomes. Specifically, the observed linear dependence between β and the asteroid's density is utilised [14]:

$$\beta = 3.61 \frac{\rho_{\text{ast}}}{2400} - 0.03 \tag{1}$$

Table 1 summarises the resulting data considered for the MKI deflection evaluation.

Diameter [m]	**Density** [kg/m^3]	**Mass** [kg]	β [-]
150.01	2244.07	$3.96677 \cdot 10^9$	3.345

Table 1: Asteroid 2024 PDC25 baseline model.

At this stage, each interaction between the spacecraft and 2024 PDC25 is assumed to have a deterministic outcome, which is then used as input for evaluating the characteristics of the subsequent spacecraft-asteroid interactions. The change in velocity imparted by each spacecraft is evaluated based on the principle of linear momentum conservation during impact, as expressed in Eq. (2) [14].

$$M_{\text{ast}} \Delta \boldsymbol{v}_{\text{ast}} = m_{\text{s/c}} \boldsymbol{V}_{\text{rel}} + m_{\text{s/c}} (\beta - 1)(\hat{\boldsymbol{E}} \cdot \boldsymbol{V}_{\text{rel}}) \hat{\boldsymbol{E}} \tag{2}$$

In the above expression, $m_{\text{s/c}}$ is the spacecraft's mass at impact, $\boldsymbol{V}_{\text{rel}}$ is the spacecraft velocity relative to the asteroid at impact, expressed in the Sun-Centred Inertial reference frame, $\hat{\boldsymbol{E}}$ denotes the direction of the ejecta plume cone's axis (assumed opposite to $\boldsymbol{V}_{\text{rel}}$), and $\Delta \boldsymbol{v}_{\text{ast}}$ represents the impact-induced variation of the asteroid's orbital velocity. The velocity variations are mapped as deviation on the b-plane by exploiting an analytically formulated State Transition Matrix (STM) [15].
The MKI model considered in this work involves spacecraft which are independently launched in sequence. As anticipated, the model is embedded into an optimisation process and the nominal mission design is subjected to operational constraints. The change in velocity is limited to 10 % to avoid fragmentation. Minimum separations of 10 and 14 days are considered for consecutive launches and impacts, respectively. Spacecraft masses are compatible with the selected launcher: the Falcon 9 Heavy [16].

	Departure	**DSM**	**Impact**	$m_{\text{s/c}}$ [kg]	$\Delta \boldsymbol{v}_{\text{ast}}^{\text{TNH}}$ [mm/s]	$\|\Delta \boldsymbol{v}_{\text{ast}}\|$	$\boldsymbol{b}^*$ [km]
s/c 1	28 April 2030	24 April 2031	05 October 2032	713.58	$\begin{bmatrix} -4.9637 \\ -3.0320 \\ -1.4312 \end{bmatrix}$	6.87% v_{esc}	$\begin{bmatrix} 3.626 \\ -5696.930 \end{bmatrix}$
s/c 2	10 May 2030	04 May 2031	22 October 2032	1126.02	$\begin{bmatrix} -7.1434 \\ -2.3660 \\ -2.8457 \end{bmatrix}$	9.58% v_{esc}	$\begin{bmatrix} 3.618 \\ -14578.650 \end{bmatrix}$
s/c 3	21 May 2030	30 May 2031	07 November 2032	794.53	$\begin{bmatrix} -5.1144 \\ 0.6221 \\ -2.3490 \end{bmatrix}$	6.74% v_{esc}	$\begin{bmatrix} 4.763 \\ -20955.895 \end{bmatrix}$

Table 2: Three-spacecraft MKI maximum impact parameter mission main features.

The minimum number of spacecraft required for the nominal design is three. Results are summarised in Table 2. As expected, optimal deflection is achieved by applying a quasi-tangential impulse close to the pericentre.

3.2. Uncertainties' analysis for MKI mission design

The identified three-spacecraft solution is selected as the baseline for the design of an MKI mission capable of responding robustly to the variation of physical and kinematic parameters.
To this aim, a Monte Carlo (MC) analysis is employed to address the effects of uncertain physical and kinematic parameters on the final deflection and the impulse magnitudes.
The uncertainties associated with the quantities reported in Table 3 are considered for this purpose.

Uncertainty source	**Variables involved**	**Number of samples**
Observations for orbit determination	Asteroid's position at first impact: $\boldsymbol{r}_{\text{imp}}$	$100,000$
Relative navigation system	Relative velocity at impacts: $\boldsymbol{V}_{\text{rel}}$	200
	Impact location on the surface: $\boldsymbol{r}_{\text{c}}$	$1,000$
Observations for physical properties	Asteroid's mass: M_{ast}	$5,000$
	Momentum enhancement factor: β	200

Table 3: Monte Carlo simulations settings.

A solution is considered robust if it satisfies both the minimum impact parameter requirement and the asteroid fragmentation threshold, each with a 2σ confidence level.

Observations for orbit determination. The covariance matrix associated with 2024 PDC25 position vector in the Sun Centred Equatorial Inertial (SCEI) reference frame at the time of the first impact is reported in Eq. 3, based on the work by D. Farnocchia shared during internal SMPAG discussion. This matrix serves as the starting point for the generation of the $N_{\text{pos}} = 100,000$ Gaussian distributed samples.

$$P_0 = \begin{bmatrix} 53.50 & -167.62 & -57.00 \\ -167.62 & 662.62 & 161.36 \\ -57.00 & 161.36 & 93.30 \end{bmatrix} \text{km}^2 \tag{3}$$

The MC analysis is performed by considering the nominal deflection of each spacecraft, applied to a random sample extract from the position error ellipsoid of the asteroid. All realisations satisfy both southward deflection and fragmentation constraints, as it can be noted from the representation of the possible deviations reported in Figure 2. As a consequence, the baseline solution is assessed to respond robustly to perturbations of the initial position of the asteroid.

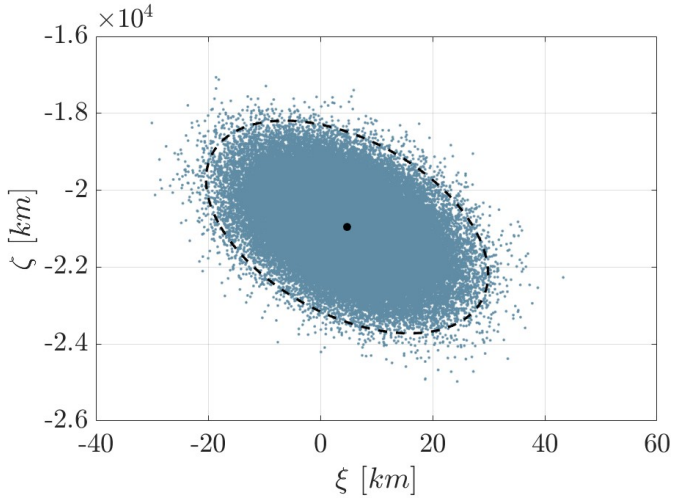

Figure 2: Impact parameter variation due to asteroid's position uncertainty for MKI nominal mission.

Relative navigation system: relative velocity at impacts. When relative navigation uncertainty is taken into account, each velocity change associated with a position sample is subjected to uncertainty. The dependence on the navigation's system accuracy is modelled considering the diagonal 3×3 covariance matrix P_{nav} expressed in the SCEI reference frame [17].

$$P_{\text{nav}} = \begin{bmatrix} 100^2 & 0 & 0 \\ 0 & 100^2 & 0 \\ 0 & 0 & 100^2 \end{bmatrix} \text{m}^2/\text{s}^2$$

Each element of the matrix represents the variance associated with any component of the relative velocity and allows for the generation of $N_{\text{nav}} = 200$ Gaussian-distributed samples ($\delta \boldsymbol{V}_{\text{rel}_{\text{nav}}}$), whose components are independent one from another.
Once the samples are generated, they are used to compute the corresponding samples associated with the uncertainty in the impact-induced asteroid's velocity change. Because the position of the asteroid is updated based on the sampled navigation error, the position error grows at every impact. With the three spacecraft considered for the baseline solution, this results in the 200^3 possible values for the impact parameter, progressively displayed in Figure 3.

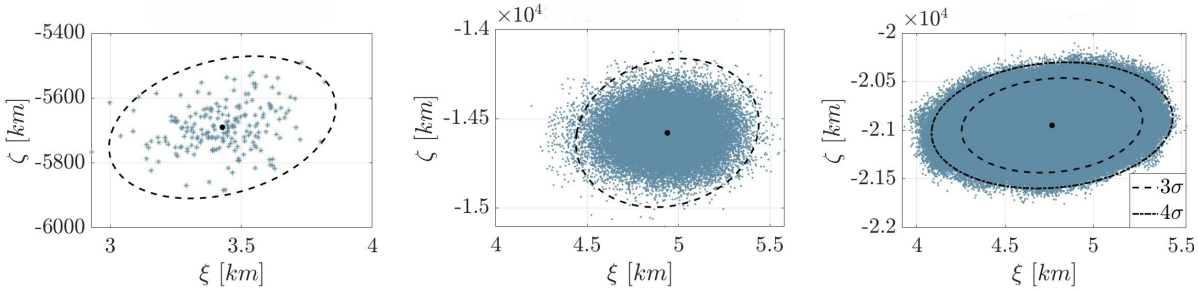

(a) First spacecraft (b) Second spacecraft (c) Third spacecraft

Figure 3: Impact parameter variation due to relative velocity uncertainty for MKI nominal mission.

None of the samples fail to meet the robustness criteria, neither for the minimum impact parameter nor for the fragmentation requirements. An increase of almost 200 km in the uncertainty associated with the component of the impact parameter along the time axis is registered for each spacecraft.

Relative navigation system: impact location on asteroid's surface. In the proposed nominal Multiple Kinetic Impactor model, the velocity change is calculated by assuming that the relative velocity between the asteroid and the impactor spacecraft is directed towards the centre of mass of 2024 PDC25. An additional assumption is made regarding the asteroid's rotational state: 2024 PDC25 is preliminarily considered to be non-rotating.
In this section we investigate the effects of different impact locations on the asteroid's surface because of relative navigation errors. The asteroid is now assumed to rotate around its axis of maximum moment of inertia [18] [19] with an assigned rotational period of 3 hours [12]. The misalignment effects are addressed in terms of overall $||\boldsymbol{\Delta v}_{\text{ast}}||$ achieved and impact parameter. The orientation of the spin axis with respect to the SCEI frame is identified by its right ascension ($\alpha_{\text{s}} = 253°$) and declination ($\delta_{\text{s}} = 74°$). Moreover, the effective ellipsoidal shape of the asteroid is considered, with its semi-axes defined as: $a_{\text{ast}} = 59.5$ m, $b_{\text{ast}} = 122$ m, and $c_{\text{ast}} = 58.5$ m.
Considering all the feasible impact locations on the asteroid's surface (namely, those visible to the spacecraft given its incoming relative direction) leads to different outcomes for the resulting velocity change $\boldsymbol{\Delta v}_{\text{ast}}$ due to the different effect associated with the ejecta mass sputtering. To this aim, the asteroid surface is discretised into N_{r} different impact locations by exploiting ellipsoidal coordinates. The ejecta mass depends on the relative orientation between the spacecraft's arrival velocity and the normal to the discrete surface element being impacted. Therefore, for each discretised element, the incidence angle is evaluated, and the corresponding ejecta mass is retrieved from the Impact and Explosion Crater Database, utilising the Holsapple-Housen web tool [20].

For this analysis, only the propagation of the effect caused by the first impactor is quantitatively analysed to determine the variation of the impact parameter in terms of order of magnitude. This

is because, after the first impact, the asteroid is likely to modify its angular velocity and establish a tumbling motion, preventing a direct mapping of the impact location's effect on the b-plane deflection. However, this condition has not yet been modelled.

Figure 4 clearly illustrates the dependence of the variation of velocity on the impact location on the surface of asteroid 2024 PDC25. The figure presents both the relationship between the ellipsoidal coordinates and the variation in the norm of the impact-induced velocity change (on the left), and a direct mapping between the cratering point and the variation of the norm of the achieved impact parameter with respect to its nominal value (on the right). Notably, the overall velocity change is affected asymmetrically by the contribution of the ejecta's tangential velocity due to the asteroid's rotation, with the magnitude differing between enhancement and reduction cases. This is a consequence of the orientation of the ejecta velocity with respect to the relative velocity between the asteroid and the spacecraft and may differ if a different mission design is considered.

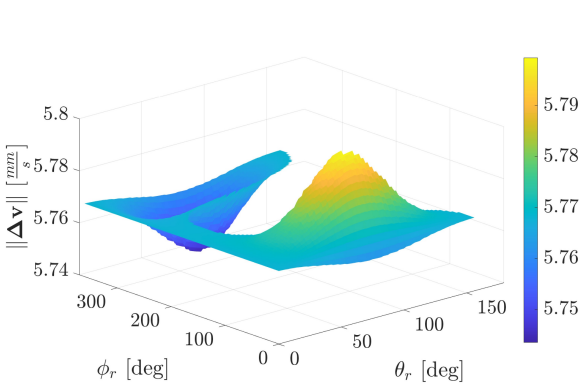

(a) Relative velocity variation with polar and azimuthal angles.

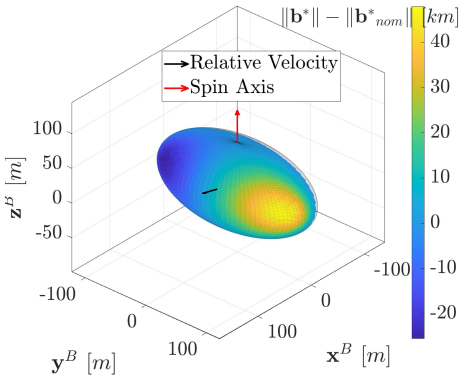

(b) Impact parameter variation with respect to the nominal value.

Figure 4: Variations due to impact location uncertainty.

The designed mission appears to behave robustly with respect to the perturbations considered in this section, as both the velocity increment and the impact parameter variation are such that the fragmentation threshold and the minimum impact parameter requirement are still met.

Observations for physical properties. Variations in the physical characteristics result in different impact parameters and, eventually, different surface escape velocities, yielding different requirements for the mission's robustness assessment.

Given the $N_{\text{ph}} = 5000$ possible physical realisations of 2024 PDC25, the difference in the achieved impact parameter compared to that corresponding to the asteroid's mean properties is evaluated. Each physical realisation is defined by a specific density, equivalent diameter, and mass. Moreover, for each density, N_β values for the momentum enhancement factor are considered, based on the 1σ uncertainty associated with the empirical relation between the momentum enhancement factor and the asteroid's density reported in Eq. (4) [14].

$$\beta = (3.61 \pm 0.2)\,\frac{\rho_{\text{ast}}}{2400} - 0.03 \pm 0.02 \quad (1\sigma) \tag{4}$$

This procedure yields the distribution in Figure 5,where the the red dots mark the realisations that exceed 10 % of the escape velocity for the second impactor, not respecting the fragmentation constraints. Quantitatively, the results show that the second spacecraft represents the most critical condition, with 39.76% of the samples not respecting the fragmentation avoidance limit. This is a consequence of the fact that a mass decrement implies a reduction of the asteroid's surface escape velocity, while also yielding an increase in the velocity variation that the impactor provides to 2024 PDC25.
As an outcome, the three-spacecraft optimal maximum impact parameter mission can not be considered a robust alternative when variability of 2024 PDC25's physical parameters is taken into account.

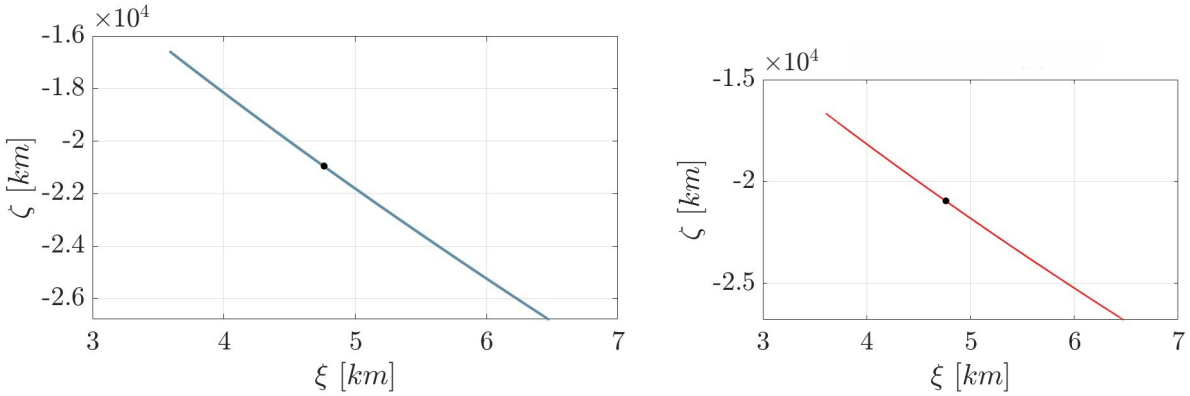

(a) Possible impact parameters arising from different physical samples.

(b) Samples for which the fragmentation threshold is not respected for the second spacecraft.

Figure 5: Impact parameter variation with physical properties.

3.3. Robust MKI mission design

Modifications to the baseline mission must be considered in order to identify a MKI solution capable of performing robustly across all the uncertainty sources taken into account. A robust solution can be identified by scaling the optimisation constraint relative to the maximum possible impact-induced velocity change, to ensure that the 10% escape velocity threshold is maintained for cases where momentum enhancement factors reach values up to 6, including also a 30 % margin.
A mission involving six spacecraft ensures that 100% of the physical realisations comply with the fragmentation limit and guarantees that 97.95% of the physical realisations meet the minimum impact parameter requirement. Robustness is achieved by employing spacecraft with smaller launch masses, which allow respecting the fragmentation requirement while still leveraging the optimal trajectory design. The mission design is summarised in Table 4, while impact locations are displayed in Figure 6.
For this particular solution, some refinements of the bounds associated with the optimisation variables were needed for such a mission design. In particular, the minimum separation between launches was reduced to three days.

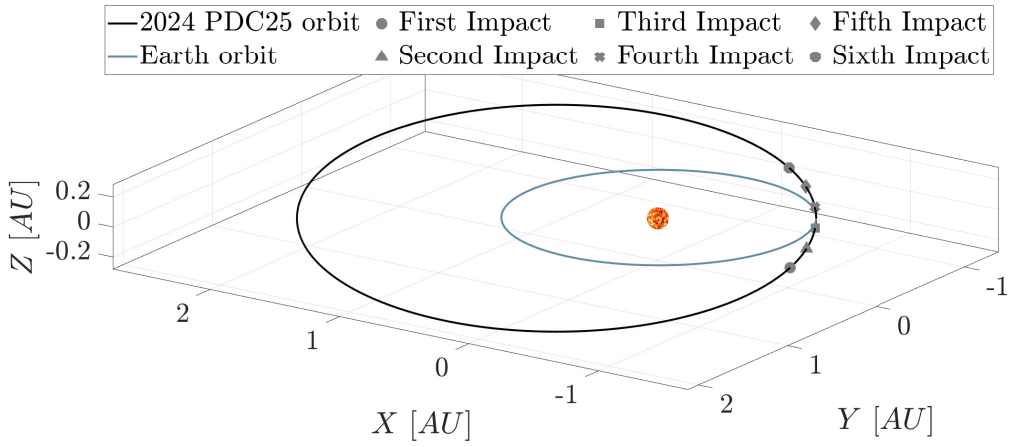

Figure 6: Impacts location along the asteroid's trajectory for the robust MKI strategy.

	Departure	DSM	Impact	$m_{s/c}$ [kg]	$\Delta \boldsymbol{v}_{ast}^{TNH}$ [mm/s]	$\|\Delta \boldsymbol{v}_{ast}\|$	$\boldsymbol{b}^*$ [km]
s/c 1	19 April 2030	21 April 2031	27 September 2032	288.89	$\begin{bmatrix} -2.0026 \\ -1.7211 \\ -0.4090 \end{bmatrix}$	3.18% v_{esc}	$\begin{bmatrix} 2.555 \\ -2387.056 \end{bmatrix}$
s/c 2	23 April 2030	15 April 2031	11 October 2032	453.84	$\begin{bmatrix} -2.8894 \\ -1.4346 \\ -0.5254 \end{bmatrix}$	3.89% v_{esc}	$\begin{bmatrix} 3.953 \\ -5932.88 \end{bmatrix}$
s/c 3	28 April 2030	14 April 2031	25 October 2032	440.30	$\begin{bmatrix} -1.6884 \\ 2.1139 \\ -1.2398 \end{bmatrix}$	3.54% v_{esc}	$\begin{bmatrix} 4.305 \\ -9485.468 \end{bmatrix}$
s/c 4	03 May 2030	17 May 2031	08 November 2032	451.57	$\begin{bmatrix} -1.4367 \\ 2.2438 \\ -1.3350 \end{bmatrix}$	3.55% v_{esc}	$\begin{bmatrix} 4.580 \\ -13022.296 \end{bmatrix}$
s/c 5	07 May 2030	15 May 2031	22 November 2032	310.99	$\begin{bmatrix} -0.4816 \\ 2.6452 \\ -1.0204 \end{bmatrix}$	3.42% v_{esc}	$\begin{bmatrix} 6.872 \\ -15656.365 \end{bmatrix}$
s/c 6	11 May 2030	10 June 2031	06 December 2032	218.36	$\begin{bmatrix} -1.5867 \\ 1.3553 \\ -0.2836 \end{bmatrix}$	2.51% v_{esc}	$\begin{bmatrix} 8.725 \\ -17549.153 \end{bmatrix}$

Table 4: Robust MKI mission main features.

The remainder 2.05% of physical realisations fail to meet the minimum impact parameter requirement. These realisations result from a high asteroid mass associated with a low momentum enhancement factor; both these characteristics represent very unlikely extremes of the probability space, enforcing the likelihood of a successful mission, supporting the choice of a 2σ confidence level for assessing mission robustness.
The six-spacecraft mission is a robust alternative for 2024 PDC25's threat mitigation. This MKI mission also enables the exploitation of successive pericenter passages of the asteroid to iteratively refine the deflection, should the effective impact parameter fall outside the bounds predicted by the simulations conducted in this study. This flexibility supports the decision not to design additional MKI campaigns at this stage, as such follow-up missions can be planned at a later time based on the outcomes of the primary campaign.

The mission design incorporates various sources of uncertainty, relying on models established in previous research. However, selecting different models may lead to variations in key design parameters. This is particularly relevant in the case of the momentum enhancement factor, whose value remains difficult to predict through empirical observations or numerical simulations. As a consequence, alternative deflection strategies are considered. Even if characterised by a lower TRL, they are, in general, less sensitive to the asteroid's physical properties and still viable for near-term implementation.

4. Mission design for rendezvousing deflection strategies

4.1. Mission optimisation process

Differently from the MKI strategy, which exploits an impulsive trajectory design to reach the asteroid, the remaining deflection strategies analysed in this work require to rendezvous with the target to perform the deflection operations. Therefore, within the optimisation process a computationally efficient shape-based low-thrust trajectory [21] is integrated with one of these deflection strategies models. For the rendezvousing strategies, the global search of solutions through the genetic algorithm is the first stage of the performed mission design. Once obtained the Pareto front, among its solutions the one maximising the deflection on the b-plane of the close encounter is selected. The key parameters from the shape-based low-thrust trajectory of the extracted mission, including the departure date, the spacecraft total mass at launch m_{s/c_0}, the excess energy provided by the launcher, and the time of flight, are used to refine the initial guess for the co-states and arrival time in the developed trajectory optimisation algorithm. Exploiting the Pontryagin Maximum Principle [22], this algorithm determines the time-optimal low-thrust trajectory to rendezvous with the asteroid while still ensuring a feasible spacecraft design.

The minimum-time option is chosen as it enables the earliest possible arrival at the NEO, which can be a great advantage especially for slow push/pull mitigation strategies, whose effectiveness directly depends on the available time to perform the deflection.

4.2. Spacecraft subsystems design

For each rendezvous deflection strategy analysed, the design of the most critical spacecraft subsystems is performed within the optimisation process. Their masses are then expressed as a percentage of the total spacecraft mass at launch, m_{s/c_0}. The sum of these percentages is subtracted from unity to determine the remaining mass available for the structure and any additional payload. To ensure mission feasibility, optimisation constraints require this remaining fraction to be greater than 13% of m_{s/c_0} and the total fuel stored on board the spacecraft to be less than 65% of m_{s/c_0}.
Given the high TRL of NEXT-C thrusters, which were employed for the DART mission [23] and in accordance with other mission analysis teams at SMPAG, these thrusters are selected for all the rendezvous missions designed in this work. Furthermore, since in each mission the spacecraft mounts multiple thrusters, they are all considered identical units. Therefore, they all share the same common properties of NEXT-C, which are reported in Table 5.

$P_{\text{in}_1,\text{max}}$ [kW]	F_{max_1} [N]	I_{sp} [s]	η_T [−]	$m_{\text{thr}_{\text{dry}}}$ [kg]
7.78	0.235	4190	0.6208	50

Table 5: NEXT-C thrusters main properties [24].

Specifically, in accordance with the NASA team at SMPAG, each NEXT-C thruster requires $P_{\text{in}_1,\text{max}} = 7.78$ kW at full power and produces a maximum thrust of $F_{\text{max}_1} = 0.235$ N. The specific impulse is selected as $I_{sp} = 4190$ s, as indicated in [24], and it is assumed constant throughout the entire mission. Consequently, to maintain these agreed properties, the corresponding thruster efficiency, also assumed constant, must be computed as shown in Eq. (5).

$$\eta_T = \frac{F_{\text{max}_1}\, I_{sp}\, g_0}{2\, P_{\text{in}_1,\text{max}}} \tag{5}$$

The solar panels sizing follows the approach in [25]. Moreover, radiators are designed to dissipate the excess power generated throughout the mission, including its peak occurring at beginning of life.

4.3. Asteroid 2024 PDC25 percentiles properties

Table 6 presents the relevant physical properties of the most representative asteroid realisations, which are extracted from the distribution provided in [12] and considered for the rendezvous deflection strategies missions. Specifically, it includes the asteroid effective spherical diameter, $d_{\text{ast}} = 2\,R_{\text{ast}}$, its bulk density, ρ_{ast}, mass, M_{ast}, and albedo, α_S. Using the first three parameters, the surface escape velocity, v_{esc}, can be computed for each case. It is worth noting that the asteroid size range at epoch 2 is around the 75^{th} percentile of the size distribution at epoch 1. However, an uncertainty factor of 3.5 in the asteroid mass still causes significant differences in deflection mission performance across the asteroid size cases considered.

Case	d_{ast} [m]	ρ_{ast} [kg/m^3]	M_{ast} [kg]	α_S [−]	v_{esc} [cm/s]
Lowest Mass	147	1211	2.00×10^9	0.221	6.05
50$^{\text{th}}$ Percentile	150	2207	3.93×10^9	0.179	8.33
Highest Mass	155	3598	7.03×10^9	0.090	10.99

Table 6: Asteroid 2024 PDC25 percentiles properties at Epoch 2 [12].

4.4. Rationale and timelines of rendezvous strategies campaigns

As described in Section 2.1, asteroid 2024 PDC25 can be deflected either northward or southward with any of the rendezvousing strategies. The following sections present solutions for both northward and southward deflection missions, expressing the achieved deviation as a percentage of the impact

risk chord length C. Specifically, for each mission designed the deflection is initially attempted in the southward direction. If the requirement is respected, the achieved deviation is highlighted in blue. If the southward requirement cannot be fulfilled, a northward deflection is attempted and, if successful, the achieved deviation is marked in orange. However, if also deflecting northward cannot prevent the asteroid impact, the best alternative would be to redirect the asteroid towards the Southern Ocean, therefore the solution indicates the corresponding partial southward deflection in red.
The campaigns presented for the rendezvousing strategies are distinguished based on their departure timing. Specifically, the early campaign involves a launch soon after the departure window opens in June 2029, providing a stringent but still feasible mission development timeline. The primary campaign launches in June 2031, the secondary campaign in May 2033, and the late one in June 2035. Finally, it is important to note that the slow push/pull deflection missions presented in this study continue until the asteroid close encounter with Earth in 2041. Therefore, the deflection performance indicated in the results is fully achieved at the hazardous MOID.

5. Stand-off NEDs in "Carrier" configuration

The developed nuclear deflection strategy exploits one or more NEDs transported to the asteroid on board a "Carrier" spacecraft. The rendezvous "Carrier" configuration allows to release the nuclear devices from a vantage observation point. The detonations occur on the far side of the asteroid with respect to the spacecraft, which is shielded from radiation and debris [5].
In the proposed model, the rendezvous with the asteroid is constrained to happen 4 - 23 months before perihelion, providing sufficient time to perform observations, collect data and prepare for deflection operations. The NEDs are detonated in the vicinity of the following perihelion, with a time separation of 14 days to allow the asteroid to recompact after each explosion. This commonly accepted interval was selected in accordance with latest results from the DART mission [2], indicating that the ejecta from Dimorphos no longer represented a threat after about two weeks from the spacecraft impact.
Following [5] and [26], the total impulsive δv_{Nuc} delivered to the asteroid by a nuclear stand-off explosion results from the consequent energy release, primarily through X-rays, neutrons, gamma radiation, and debris impacting the NEO surface. Given the greater energy release, fusion-based devices are selected, with the fractions of energy among the components retrieved from [26]. To avoid an undesired fragmentation of the asteroid, a limit must be imposed on the imparted δv_{Nuc}. The current heuristic criterion proposed by NASA, based on the analyses of the DART mission outcome [14], indicates a threshold between 4% and 10% of the asteroid surface escape velocity, v_{esc}, depending on the value of the momentum enhancement factor, β. For this strategy, a conservative assumption is adopted by setting $\beta = 2$. Accordingly, the fragmentation limit applied to each impulse is defined in Eq. (6).

$$\delta v_{\text{Nuc}} \leq 4\%\, v_{\text{esc}} \tag{6}$$

Since the stand-off detonation distance H strongly influences the δv_{Nuc} imparted to the asteroid, it is considered as an additional optimisation variable of the model. This enables the optimiser to control the imparted impulses and respect the imposed fragmentation threshold.

5.1. Missions with stand-off NEDs strategy

The optimised early, primary, secondary and late deflection missions for asteroid 2024 PDC25 using stand-off NEDs in the "Carrier" configuration are described in Table 7, where the deflection is expressed as a percentage of the impact risk chord length C. Each campaign exploits a later asteroid perihelion to perform the detonation events, consequently requiring an increasing number of devices to ensure the deflection of the asteroid, at least northward, across all the considered size cases. To accommodate an increased number of NEDs onboard, a corresponding decrease in the yield per device is required to ensure spacecraft design feasibility. Reducing the charge of each device is not an issue, as the fragmentation threshold already limits the maximum impulse that can be delivered. Additionally, the stand-off detonation distance, H, introduced as an optimisation variable, can be adjusted by the optimiser to deliver an impulse as close as possible to the fragmentation threshold, to maximise the deflection. The maximum number of devices needed to deflect the asteroid even at the last useful perihelion before the close encounter with Earth is thirteen, each with a charge of 0.2 Mt. Future studies should investigate the potential benefits of deploying even more devices, each with a lower yield of 0.1 Mt.

	Early (2032 Perihelion)		Primary (2034 Perihelion)		Secondary (2037 Perihelion)		Late (2039 Perihelion)
	5 x 0.4 Mt	**7 x 0.3 Mt**	**5 x 0.4 Mt**	**7 x 0.3 Mt**	**7 x 0.3 Mt**	**9 x 0.3 Mt**	**13 NEDs x 0.2 Mt**
m_{s/c_0} [kg]	10754.72	10813.41	10775.73	10819.65	10377.72	10871.90	11170.07
Lowest Mass	73.03	101.95	52.94	76.76	51.14	64.65	41.25
50th percentile	101.91	140.81	76.59	105.34	70.29	88.89	56.77
Highest Mass	134.56	185.82	101.05	139.52	92.70	115.24	74.83

Table 7: Stand-off nuclear deflection campaigns for asteroid 2024 PDC25.

The fragmentation limit, imposed directly on the imparted impulse and defined as a small percentage of the asteroid's surface escape velocity, also explains the counter-intuitive result of larger deflection achieved for larger asteroid size cases. Higher-mass asteroids are characterised by a greater escape velocity, which allows the application of stronger impulses while still respecting the imposed fragmentation threshold, resulting in a larger deflection compared to lower-mass asteroid cases.

6. Single and Multiple Ion Beam Deflection

Following the Ion Beam Deflection (IBD) concept proposed in [10], the spacecraft is oriented such that the ion beam from the primary thruster impinges entirely on the asteroid, transferring momentum that gradually alters its orbit. Meanwhile, the nominal position of the spacecraft is maintained by symmetric firing of the opposing secondary ion thruster. This study implements two methods to enhance the effectiveness of the IBD strategy. The spacecraft can be equipped with multiple pairs of identical ion thrusters and more spacecraft can be considered to simultaneously target the asteroid with ion beams from different positions. Therefore, the additional optimisation variables for the IBD models are the integer number of thruster pairs on each spacecraft, N_{pairs}, and the integer number of spacecraft, $N_{s/c}$.
Multiple spacecraft must be properly spaced to prevent interfering with each other. This can be achieved by placing them in formation flight with the asteroid on a periodic orbit. However, a key consideration in this setup is the partial cancellation of the deviation force exerted by multiple IBD spacecraft evenly spaced on a formation orbit, applying thrust from opposing directions. While this reduces the net acceleration imparted to the asteroid, results demonstrate that the MIBD strategy in formation flight still achieves significantly better deflection performance than a single IBD spacecraft. The formation orbits design ensures that each spacecraft remains within the maximum distance at which its ion beam fully intercepts the asteroid surface. Simultaneously, the spacecraft must not be too close to the asteroid. In fact, the closer they are, the larger is the contribution of deviation force cancelling out and the stronger is the back-sputtering effect.
The instantaneous perturbing force experienced by the asteroid expressed in the local TNH reference frame, $\boldsymbol{F}_{\text{dev}}^{\text{TNH}}(t)$, is equal and opposite to the total force exerted by the primary thrusters on the spacecraft, as reported in Eq. (7).

$$\boldsymbol{F}_{\text{dev}}^{\text{TNH}}(t) = -N_{\text{pairs}} \sum_{i=1}^{N_{\text{s/c}}} \boldsymbol{F}_{p_1,i}^{\text{TNH}}(t) \tag{7}$$

Where $\boldsymbol{F}_{p_1,i}^{\text{TNH}}(t)$ is the instantaneous force vector produced by one primary thruster of each spacecraft, also expressed in the local TNH reference frame centred at the asteroid.
In the single IBD model ($N_{\text{s/c}} = 1$), the spacecraft hovers in a position always aligned with the asteroid velocity vector, either ahead or behind it depending on the direction of the desired deflection. Consequently, the force produced by the primary thrusters is assumed to act along the tangential direction of the asteroid heliocentric orbit. In the MIBD strategy, the total deviating force produced by the primary thrusters, considering all pairs, N_{pairs}, and all spacecraft simultaneously performing the deflection, $N_{\text{s/c}}$, accounts for the different firing directions of each spacecraft in the formation orbit. The perturbing acceleration exerted on the asteroid by the Single or Multiple IBD spacecraft, $\boldsymbol{a}(t) = \boldsymbol{a}_{\text{IBD}}^{\text{TNH}}(t)$, is obtained by dividing the instantaneous perturbing force by the asteroid mass, M_{ast}.
As for the LA strategies, also in the IBD case the negative tugging contribution is taken into account. Therefore, the total perturbing acceleration, $\boldsymbol{a}(t)$, used in Gauss' planetary equations to compute the IBD deflection, also considers the tugging acceleration, $\boldsymbol{a}_{\text{tug}}(t)$ expressed in the TNH reference frame, as shown in Eq. (8).

$$\boldsymbol{a}(t) = \boldsymbol{a}_{\text{IBD}}^{\text{TNH}}(t) - \boldsymbol{a}_{\text{tug}}(t) \tag{8}$$

As the asteroid moves away from the Sun towards its aphelion, where the deflection is least effective, the decreasing available power reduces the produced thrust, further diminishing the deflection performance. To avoid inefficient fuel expenditure, the SIBD and MIBD models developed in this work allow the thrusters to throttle down to half power, deactivating them when the available power per thruster falls below this threshold. As a result, the deflection action is performed in arcs around each asteroid perihelion and it is suspended while moving towards the aphelion.

6.1. Single and Multiple Ion Beam Deflection missions

The optimised early, primary and secondary campaigns to deflect asteroid 2024 PDC25 with the Single and Multiple IBD strategies are reported in Table 8. The approach adopted in these missions design is to determine the minimum number of spacecraft needed to achieve a southward deflection of the asteroid. For the smaller asteroid sizes and earlier campaigns, multiple IBD spacecraft are not required to achieve a southward deflection. Specifically, the early mission with one spacecraft ensures the deflection of the asteroid, at least northward, in all size cases. Instead, later campaigns and larger asteroid size cases need an increasing number of spacecraft to achieve a southward deflection.
Since the optimisation variable N_{pairs} can vary from 3 to 6, the genetic algorithm explores feasible spacecraft configurations for all acceptable thruster pair values, leading to different deflection performances in the Pareto front. Because the mission extracted from the Pareto front is the one achieving maximum deflection, all the optimised mission options presented for this strategy employ the maximum allowed number of thruster pairs, that is $N_{\text{pairs}} = 6$. This corresponds to a power requirement at 1 AU of 93.36 kW. Table 8 also highlights the large spacecraft mass required at launch for the IBD strategy, mostly due to the significant amount of fuel needed to perform the deflection action.

	Early - Launch June 2029			**Primary - Launch May 2031**			**Secondary - Launch June 2033**		
	m_{s/c_0} [kg]	$N_{s/c}$ [−]	$\|\|\boldsymbol{b}^*\|\|$ [% C]	m_{s/c_0} [kg]	$N_{s/c}$ [−]	$\|\|\boldsymbol{b}^*\|\|$ [% C]	m_{s/c_0} [kg]	$N_{s/c}$ [−]	$\|\|\boldsymbol{b}^*\|\|$ [% C]
Lowest Mass	12171.07	**1**	153.75	10651.21	**1**	114.00	11920.59	**3**	127.82
50$^{\text{th}}$ percentile	12416.02	**1**	74.26	10304.53	**2**	102.69	10475.57	**4**	79.32
Highest Mass	12413.23	**2**	76.11	10680.19	**3**	80.53	10427.69	**6**	98.68
	12176.69	**1**	36.26						

Table 8: IBD deflection campaigns for asteroid 2024 PDC25.

It is worth mentioning the reduction of fuel amount per spacecraft required by a secondary IBD mission, which loses two perihelia arcs compared to the early mission and one perihelion arc compared to the primary mission to accomplish the deflection. Conversely, due to its high fuel requirement, the spacecraft design for the IBD early mission is the closest among all strategies to the constraint on the structure and any additional payload mass fraction being larger than 13% of m_{s/c_0}.

7. Single and Multiple Laser Ablation

The Laser Ablation (LA) model developed in this work follows the one presented in [8] and [9]. Since asteroid 2024 PDC25 is confirmed to be an S-type [12], the assumed material is forsterite $(\text{Mg}_2\text{SiO}_4)$, a common variety of olivine, typically used to represent the composition of S-type asteroids. The instantaneous perturbing acceleration imparted to the asteroid is expressed in Eq. (9), in which the asteroid mass decreases in time due to the sublimated material expelled from its surface. The product of the ejecta velocity, $\bar{v}$, and the instantaneous sublimated material mass flow rate, $\dot{m}_{sub}(t)$, provides the instantaneous force acting on the asteroid, $F_{sub} = S_{sc}\,\bar{v}\,\dot{m}_{sub}(t)$. The parameter $S_{sc} = 2/\pi$ is the scattering factor of the ejecta plume, assumed constant.

$$a_{sub}(t) = \frac{S_{sc}\,\bar{v}\,\dot{m}_{sub}(t)}{M_{\text{ast}}(t)} \tag{9}$$

The sublimation acceleration is assumed to be aligned with the instantaneous tangential direction of the asteroid heliocentric orbit, therefore it is expressed in the TNH reference frame as $\boldsymbol{a}_{sub}(t) = [a_{sub}(t)\ 0\ 0]^T$. In the Single LA configuration, the spacecraft maintains a stable hovering position, aligned with the

tangential direction of the asteroid heliocentric orbit. The hovering distance is an additional optimisation variable that significantly affects the deflection performance. In fact, the ablated material is assumed to permanently deposit on exposed sensitive surfaces, such as solar panels, accumulating over time and gradually reducing the solar array power output, which in turn decreases the ablation system performance [9]. Therefore, achieving substantial deflection with a single spacecraft would require an impractically high-power laser system. An alternative approach proposed in [27] involves one or more spacecraft flying in formation with the asteroid. This configuration avoids low elevation angle regions, characterised by a higher density of the ejecta plume. As a result, it reduces the degradation of the laser system throughout the mission by limiting the accumulation of ejecta material on sensitive surfaces.
In this work, the formation orbits design follows the one reported in [28]. The spacecraft in close proximity of the asteroid exert a gravitational pull on it, which is a negative tugging contribution to the overall pushing effect produced by the ablation process. Therefore, the total perturbing acceleration to be used in the Gauss' planetary equations, reported in Eq. (10), also considers the tugging acceleration expressed in the local TNH reference frame centred at the asteroid, $\boldsymbol{a}_{\text{tug}}(t)$.

$$\boldsymbol{a}(t) = \boldsymbol{a}_{sub}(t) - \boldsymbol{a}_{\text{tug}}(t) \tag{10}$$

The laser power requirement at 1 AU, $P_{L_{1AU}}$, is introduced as an additional optimisation variable reaching up to 91 kW, a limit imposed by the sizing of solar panels, which become impractically large at higher power levels. With this high power demand, each spacecraft requires a dedicated launch. However, cost is not expected to be a main driver for an asteroid impact threat scenario, therefore this design strategy is exploited to achieve better deflection performance for asteroid 2024 PDC25.

7.1. Single and Multiple Laser Ablation missions

For the single LA strategy, only two variations of the early deflection campaign are considered, as later launches of one spacecraft yield insufficient deflection performance due to the power limitations adopted in this study. In contrast, deploying multiple LA spacecraft in formation flight with the asteroid significantly improves deflection performance, enabling the feasibility of early, primary, and secondary deflection campaigns.
The two early campaigns for the single LA strategy are reported in Table 9. The key difference between them lies in the hovering distance range. In fact, with the model developed in this work, hovering closer to the asteroid leads to a greater accumulation of deposited ejecta material on solar panels, significantly degrading their power generation capacity throughout the mission. This, in turn, reduces the efficiency of the laser ablation system and ultimately lowers the achieved deflection. Conversely, increasing the hovering distance mitigates the accumulation of deposited ejecta during the deflection process. Although the spacecraft remains at zero elevation angle, where the plume density is highest for a fixed distance from the illuminated spot, a greater distance results in a lower overall ejecta plume density. This helps sustain a higher laser system efficiency over time, leading to greater deflection performance. Specifically, the larger hovering distance option allows a southward deflection in the Lowest Mass case and a northward deflection for the 50$^{\text{th}}$ percentile. Conversely, the lower hovering distance campaign fails to prevent the asteroid impact, regardless of its size.

	Early campaign - Launch June 2029							
	Low hovering distance				**High hovering distance**			
	m_{s/c_0} [kg]	d_{hover} [m]	$P_{L_{1AU}}$ [kW]	$\|\|\boldsymbol{b}^*\|\|$ [% C]	m_{s/c_0} [kg]	d_{hover} [m]	$P_{L_{1AU}}$ [kW]	$\|\|\boldsymbol{b}^*\|\|$ [% C]
Lowest Mass	8321.96	526.47	90.00	29.91	8401.83	1127.68	90.29	74.01
50$^{\text{th}}$ percentile	8771.85	443.92	90.51	10.93	9269.89	1154.30	90.26	35.65
Highest Mass	8608.10	535.83	90.67	8.14	9244.37	1178.60	90.43	19.35

Table 9: SLA deflection campaigns in hovering configuration for asteroid 2024 PDC25.

A strong improvement in deflection performance is achieved when considering the formation flight configuration, which proved to be highly advantageous even when using a single LA spacecraft. In fact, as shown in Table 10, one spacecraft operating in formation flight with the asteroid is sufficient to achieve a southward deflection in the Lowest Mass and 50$^{\text{th}}$ percentile cases of the early campaign,

as well as in the Lowest Mass case of the primary campaign. For later missions and larger asteroid size cases, an increasing number of spacecraft is required to ensure a southward deflection, reaching a maximum of four in the Highest Mass case of the secondary campaign. This value is lower than the corresponding maximum number of spacecraft required in the IBD campaigns. However, this is primarily due to the high power levels considered for the laser ablation system, and the partial cancellation of the net thrust applied to the asteroid affecting the deflection performance of the MIBD strategy.

	Early - Launch July 2029			**Primary - Launch May 2031**			**Secondary - Launch May 2033**		
	$P_{L_{1AU}}$ [% C]	$N_{s/c}$ [−]	$\|\|\boldsymbol{b}^*\|\|$ [% C]	$P_{L_{1AU}}$ [kW]	$N_{s/c}$ [−]	$\|\|\boldsymbol{b}^*\|\|$ [% C]	$P_{L_{1AU}}$ [kW]	$N_{s/c}$ [−]	$\|\|\boldsymbol{b}^*\|\|$ [% C]
Lowest Mass	86.78	**1**	154.71	89.26	**1**	126.43	88.74	**2**	133.90
50th percentile	86.92	**1**	78.83	89.56	**2**	118.21	89.86	**3**	99.28
Highest Mass	87.10	**2**	89.57	88.78	**3**	104.54	89.50	**4**	76.16

Table 10: MLA deflection campaigns in formation flight with asteroid 2024 PDC25.

8. Standard and Enhanced Gravity Tractor

The standard Gravity Tractor model developed in this work follows the hovering configuration proposed in [6]. This slow-pull technique exploits the mutual gravitational attraction between the NEO and the spacecraft to apply a small but continuous perturbing acceleration, which is reported in Eq. (11).

$$a_{\mathrm{GT}}(t) = \frac{G\, m_{s/c}(t)}{d_{\mathrm{hover}}^2} \tag{11}$$

Where d_{hover} is the hovering distance, $m_{s/c}(t)$ is the instantaneous spacecraft mass, decreasing due to the consumption of fuel needed for hovering, and G is the universal gravitational constant.
The Enhanced Gravity Tractor improves the standard GT technique by collecting mass from the asteroid surface to increase the spacecraft mass and enhance the gravitational attraction [7]. This work accounts for the material collection with an additional fuel allowance equal to 5% of m_{s/c_0} and a one-month period after rendezvousing with the asteroid to acquire $M_{\mathrm{gain}} = 50 \times 10^3$ kg, before starting the deflection process. The instantaneous perturbing acceleration imparted by the EGT spacecraft is expressed in Eq. (12), where $d_{\mathrm{hov,EGT}}$ is the hovering distance of the EGT spacecraft, which increases with respect to the GT case due to the larger spacecraft mass. The parameter $m_{s/c,\mathrm{EGT}}(t) = m_{s/c}(t) + M_{\mathrm{gain}}$ follows the same decreasing law of the GT strategy, but with the spacecraft mass augmented of 50 tons and the asteroid mass reduced by the same amount.

$$a_{\mathrm{EGT}}(t) = \frac{G\,[m_{s/c}(t) + M_{\mathrm{gain}}]}{d_{\mathrm{hov,EGT}}^2} \tag{12}$$

Similarly to the LA models, the acceleration imparted by the GT and EGT is assumed aligned with the instantaneous tangential direction of the asteroid heliocentric orbit.

8.1. Standard and Enhanced Gravity Tractor missions

For the GT and EGT strategies, only the early and primary campaigns are proposed in Table 11, as later missions do not provide sufficient warning time to achieve a significant deflection of asteroid 2024 PDC25. The standard GT option proves largely ineffective for this scenario. Even in the early campaign, it fails to achieve a southward deflection in any of the asteroid size cases analysed. A northward deflection is possible in the early mission for the Lowest Mass and 50th percentile cases, while in the primary mission it is only feasible for the Lowest Mass case.
The EGT strategy significantly improves deflection performance compared to the standard GT. In the early EGT campaign, a southward deflection is achieved for the Lowest Mass case, while a northward deviation is possible for the other two cases. In the primary mission, the Lowest Mass case can still be deflected southward, the 50th percentile allows for a northward deviation, whereas for the Highest Mass case, the impact cannot be prevented.

	Early campaign - Launch June 2029				Primary campaign - Launch June 2031			
	Standard GT		Enhanced GT		Standard GT		Enhanced GT	
	d_{hover} [m]	$\|\boldsymbol{b}^*\|$ [% C]	$d_{\text{hov,EGT}}$ [m]	$\|\boldsymbol{b}^*\|$ [% C]	d_{hover} [m]	$\|\boldsymbol{b}^*\|$ [% C]	$d_{\text{hov,EGT}}$ [m]	$\|\boldsymbol{b}^*\|$ [% C]
Lowest Mass	85.74	51.49	147.17	124.32	85.29	31.75	148.74	80.52
50$^{\text{th}}$ percentile	99.69	37.40	196.92	68.05	98.99	22.26	195.36	45.51
Highest Mass	119.95	24.87	256.70	40.70	122.20	17.28	255.07	26.78

Table 11: Standard and Enhanced GT deflection campaigns for asteroid 2024 PDC25.

The hovering distance for the EGT strategy is larger compared to that of the standard GT strategy for the corresponding asteroid size percentiles. This outcome is expected, as the gravitational attraction increases significantly with the addition of M_{gain} to the spacecraft mass. As a result, the two thrusters operating at full power are unable to maintain a closer hovering position.
Because of the additional fuel demand for the mass collection operations and for hovering with an augmented spacecraft mass, the EGT strategy requires a fuel amount comparable to that of IBD missions, yet the latter offers superior deflection performance. Furthermore, it is worth mentioning that the mass collection subsystem was not explicitly designed, as it falls outside the scope of this work. However, all EGT missions allocate sufficient mass for the structure and non-modelled subsystems, including the collection mechanisms.

9. TRL considerations and preferred strategies

The GT strategy has a relatively high TRL, as it requires a spacecraft to simply hover near the asteroid. However, its performance to deflect asteroid 2024 PDC25 is very low given the warning time available. The EGT improves deflection performance, but adds complexity to the mission architecture due to the uncertainty and low TRL of the mass collection system. Furthermore, differently from the GT, the EGT is affected by the asteroid properties and composition. Given these limitations, the gravity tractor strategies can be ruled out as viable options to deflect asteroid 2024 PDC25.
The SLA strategy does not achieve sufficient deflection of the asteroid. However, using multiple laser ablation spacecraft in a formation flight configuration significantly improves deflection performance. With the considered laser system power levels, MLA requires fewer spacecraft than MIBD to ensure a southward deflection of the asteroid. Despite this, laser ablation suffers from a lower TRL compared to ion beam deflection. In fact, laser-based deflection technologies have never been operated at the high power levels required to deflect asteroid 2024 PDC25. In contrast, IBD technology is expected to undergo flight testing in upcoming space debris removal missions. Thus, while MLA offers promising performance, IBD remains a more technically mature solution to deflect asteroid 2024 PDC25.
The MKI strategy has the highest TRL among all the considered strategies, enabling a relatively short development time. This allows for the design of a single mission capable of exploiting the asteroid's 2032 pericentre, while still granting the possibility to use successive perihelion passages. Table 12 summarises the characteristics of the effective MKI mission for asteroid 2024 PDC25 full deflection.

Launch	$N_{\text{s/c}}$ [−]	Mass in space [kg]	Perihelion	Development time
April - May 2030	6	3229	1$^{\text{st}}$ November 2032	Sufficient

Table 12: Summary of MKI mission for asteroid 2024 PDC25.

The stand-off NEDs technique is the most effective single-spacecraft strategy for deflecting asteroid 2024 PDC25, with existing technology capable of delivering as many impulses as needed. Table 13 summarises the early, primary, secondary and late stand-off NEDs deflection campaigns for asteroid 2024 PDC25. A maximum of thirteen impulses is required to fully deflect the asteroid, at least northward in all asteroid size cases, even when detonations are performed around the last useful perihelion before the close encounter one.

Mission	Launch	Mass in space [kg]	Perihelion	N_{NEDs} [−]
Early	June 2029	10754.72	1st November 2032	5
Primary	May 2031	10775.73 – 10819.65	15th December 2034	5 – 7
Secondary	June 2033	10377.72 – 10871.90	27th January 2037	7 – 9
Late	June 2035	11170.07	12th March 2039	13

Table 13: Summary of stand-off nuclear deflection campaigns for asteroid 2024 PDC25.

The feasibility of a nuclear deflection mission is limited by the lack of full-scale tests of NEDs in space, as well as significant political and legal constraints. Therefore, apart from the proposed MKI deflection mission, the most promising deflection strategy among the others analysed remains IBD, whose early, primary and secondary campaigns are summarised in Table 14.

Mission	Launch	$N_{s/c}$ [−]	Mass in space [kg]	Development time
Early	June 2029	1	12416.02	Stringent
Primary	May 2031	2 – 3	20609.06 – 30913.59	Sufficient
Secondary	June 2033	3 – 6	31426.71 – 62853.42	Extensive

Table 14: Summary of IBD campaigns to deflect asteroid 2024 PDC25.

The early IBD campaign with one spacecraft ensures a full deflection of the asteroid, at least northward, in all asteroid size cases. However, it might have a too stringent mission development timeline. Therefore, the primary campaign remains the most promising to deflect asteroid 2024 PDC25. Launching two spacecraft enables a southward deflection for the Lowest Mass and 50th percentile cases, while a northward deflection for the Highest Mass case. Instead, launching three spacecraft ensures a southward deflection also for the Highest Mass and provides redundancy if the asteroid turns out to be the smaller size cases. The secondary campaign remains a back-up or alternative mission, providing longer development time, but requiring more spacecraft to ensure a southward deflection of the asteroid.

10. Conclusion

This study has developed and optimised trajectory, reconnaissance and deflection missions to mitigate the hypothetical impact threat posed by asteroid 2024 PDC25. A robust mission design is proposed with the MKI strategy, which includes uncertainty analyses in the key parameters associated with this deflection technique. The mission design demonstrated the effectiveness of the MKI strategy in successfully deflecting asteroid 2024 PDC25, while preserving sufficient flexibility to exploit the entire warning time for additional deflection campaigns.
Less technically mature strategies also proved to be efficient in deflecting asteroid 2024 PDC25. This work also focused on implementing and improving models of deflection techniques with a lower TRL compared to the kinetic impactor, yet still feasible for near-term application with sufficient technological advancements. Specifically, these deflection strategies rely on a low-thrust trajectory to rendezvous with the asteroid, allowing for both a northward and southward deflection. As an impulsive alternative to the Kinetic Impactors, the stand-off NEDs in “Carrier” configuration proved to be the most effective single spacecraft strategy among all deflection techniques analysed. Instead, several continuous push/pull deflection strategies were deemed sufficiently advanced in TRL to be considered in this work: Single and Multiple Laser Ablation, Standard and Enhanced Gravity Tractor, and Single and Multiple Ion Beam Deflection. For the rendezvousing strategies, optimised deflection campaigns were proposed with different timelines, and a final comparison was conducted, based on their performance, technological readiness, and feasibility within the available warning time. The stand-off NEDs in “Carrier” configuration and the IBD techniques emerged as the most viable options to deflect asteroid 2024 PDC25. Nuclear deflection, while highly effective from the performance viewpoint, faces significant political and regulatory constraints that currently limit the possibility of testing nuclear devices in space. Instead, IBD balances technological and political feasibility, deflection performance and scalability, making it the optimal choice along with the MKI, under realistic TRL advancement timelines.

Acknowledgments

The research within this study is part of the European Research Council (ERC) under the European Union's Horizon Europe research and innovation program as part of the GREEN SPECIES project (Grant agreement No - 101089265). The authors would like to acknowledge Mr. Lindley Johnson, Mr. Brent W. Barbee, Dr. Paul Chodas and Dr. Davide Farnocchia for their great advice, which helped guiding the development of this work.

References

[1] NASA, NASA Confirms DART Mission Impact Changed Asteroid's Motion in Space, 2022. URL: https://www.nasa.gov/news-release/nasa-confirms-dart-mission-impact-changed-asteroids-motion-in-space/ [Accessed: 26 April 2025].

[2] N. Chabot, E. Adams, A. Rivkin, J. Kalirai, DART: Latest results from the Dimorphos impact and a look forward to future planetary defense initiatives, Acta Astronautica 220 (2024) 118–125. Doi: https://doi.org/10.1016/j.actaastro.2024.04.001.

[3] I. Bolzoni, Multiple Kinetic Impactor for Deflection of Potentially Hazardous Asteroids, Master's thesis, Politecnico di Milano, 2021.

[4] P. Hammerling, J. L. Remo, NEO interaction with nuclear radiation, Acta Astronautica 36 (1995) 337–346. Doi: https://doi.org/10.1016/0094-5765(95)00111-5.

[5] M. Vasile, N. Thiry, Nuclear cycler: An incremental approach to the deflection of asteroids, Advances in Space Research 57 (2016) 1805–1819. Doi: https://doi.org/10.1016/j.asr.2015.11.036.

[6] B. Wie, Dynamics and Control of Gravity Tractor Spacecraft for Asteroid Deflection, Journal of guidance, control, and dynamics 31 (2008) 1413–1423. Doi: https://doi.org/10.2514/1.32735.

[7] D. D. Mazanek, D. M. Reeves, J. B. Hopkins, D. W. Wade, M. Tantardini, H. Shen, Enhanced Gravity Tractor Technique for Planetary Defense, in: Proceedings of the IAA Planetary Defense Conference, Frascati, Roma, Italy. IAA-PDC-15-04-11. URL: https://ntrs.nasa.gov/citations/20150010968 [Accessed: 26 April 2025].

[8] J. P. Sanchez Cuartielles, Asteroid hazard mitigation: deflection models and mission analysis, Ph.D. thesis, University of Glasgow, 2009.

[9] M. Vasile, A. Gibbings, I. Watson, J.-M. Hopkins, Improved laser ablation model for asteroid deflection, Acta Astronautica 103 (2014) 382–394. Doi: https://doi.org/10.1016/j.actaastro.2014.01.033.

[10] C. Bombardelli, J. Peláez, Ion Beam Shepherd for Asteroid Deflection, Journal of Guidance, Control, and Dynamics 34 (2011) 1270–1272. Doi: https://doi.org/10.2514/1.51640.

[11] C. Colombo, Optimal trajectory design for interception and deflection of Near Earth Objects, Ph.D. thesis, University of Glasgow, 2010.

[12] NASA/JPL Center for Near Earth Object Studies, 2025 Planetary Defense Conference Hypothetical Asteroid Impact Scenario, 2024. URL: https://cneos.jpl.nasa.gov/pd/cs/pdc25/ [Accessed: 26 April 2025].

[13] P. Bland, N. Artemieva, Efficient disruption of small asteroids by Earth's atmosphere, Nature 424 (2003) 288–291. Doi: https://doi.org/10.1038/nature01757.

[14] A. F. Cheng, H. F. Agrusa, B. W. Barbee, A. J. Meyer, T. L. Farnham, S. D. Raducan, D. C. Richardson, E. Dotto, A. Zinzi, V. Della Corte, et al., Momentum transfer from the DART mission kinetic impact on asteroid Dimorphos, Nature 616 (2023) 457–460. Doi: https://doi.org/10.1038/s41586-023-05878-z.

[15] J. L. Gonzalo, C. Colombo, P. Di Lizia, Analytical Framework for Space Debris Collision Avoidance Maneuver Design, Journal of Guidance, Control, and Dynamics 44 (2021) 469–487. Doi: https://doi.org/10.2514/1.G005398.

[16] J. Seibert, Ula vs spacex – a detailed comparison in 2024, Space Insider (2024).

[17] A. F. Cheng, A. S. Rivkin, P. Michel, J. Atchison, O. Barnouin, L. Benner, N. L. Chabot, C. Ernst, E. G. Fahnestock, M. Kueppers, et al., AIDA DART asteroid deflection test: Planetary defense and science objectives, Planetary and Space Science 157 (2018) 104–115. Doi: https://doi.org/10.1016/j.pss.2018.02.015.

[18] J. A. Burns, V. S. Safronov, T. Gold, Asteroid Nutation Angles, Monthly Notices of the Royal Astronomical Society 165 (1973) 403–411. Doi: https://doi.org/10.1093/mnras/165.4.403.

[19] T. Henych, P. Pravec, Asteroid rotation excitation by subcatastrophic impacts, Monthly Notices of the Royal Astronomical Society 432 (2013) 1623–1631. Doi: https://doi.org/10.1093/mnras/stt581.

[20] K. A. Holsapple, Impact and explosion crater database, 2003. Available at: https://www.lpi.usra.edu/lunar/tools/lunarcratercalc/. [Accessed: 26 April 2025].

[21] K. Zeng, Y. Geng, B. Wu, Shape-based analytic safe trajectory design for spacecraft equipped with low-thrust engines, Aerospace Science and Technology 62 (2017) 87–97. Doi: https://doi.org/10.1016/j.ast.2016.12.006.

[22] L. S. Pontryagin, The Mathematical Theory of Optimal Processes, Routledge, London, 1987. ISBN: 978-2881240775.

[23] J. Brophy, S. Pellegrino, P. Lubin, et al., Non-Nuclear Exploration of the Solar System Study, Technical Report, W. M. Keck Institute for Space Studies, Pasadena, California, 2022. URL: https://kiss.caltech.edu/final_reports/NonNuclear-final-report.pdf [Accessed: 26 April 2025].

[24] R. Shastry, R. E. Thomas, G. C. Soulas, M. C. Gonzalez, M. J. Patterson, C. M. Tolbert, NASA's Evolutionary Xenon Thruster-Commercial (NEXT-C), in: Double Asteroid Redirection Test (DART) Mission, Laurel, MD. URL: https://ntrs.nasa.gov/citations/20210024276 [Accessed: 26 April 2025].

[25] J. R. Wertz, W. J. Larson, Space Mission Analysis and Design, Springer, 1999. ISBN: 978-0792359012.

[26] J. P. Sanchez, C. Colombo, M. Vasile, G. Radice, Multicriteria Comparison Among Several Mitigation Strategies for Dangerous Near-Earth Objects, Journal of Guidance, Control, and Dynamics 32 (2009) 121–142. Doi: https://doi.org/10.2514/1.36774.

[27] A. Gibbings, J.-M. Hopkins, D. Burns, M. Vasile, On Testing Laser Ablation Processes for Asteroid Deflection, in: IAA planetary defense conference, protecting Earth from asteroids: From threat to action.

[28] M. Vasile, C. A. Maddock, Design of a formation of solar pumped lasers for asteroid deflection, Advances in space research 50 (2012) 891–905. Doi: https://doi.org/10.1016/j.asr.2012.06.001.